Molecular Dynamics Simulations of Carbon Monoxide Dissociation from Heme a_3 in Cytochrome *c* Oxidase from *Paracoccus Denitrificans*

Jean-Christophe Lambry, Marten H. Vos,* and Jean-Louis Martin

INSERM U451, Laboratoire d'Optique Appliquée, Ecole Polytechnique-ENSTA, 91761 Palaiseau Cedex, France

Received: July 26, 1999; In Final Form: October 1, 1999

We have investigated ligand motions in the heme a_3−CuB binuclear active site of cytochrome *c* oxidase by molecular dynamics simulations. The starting structural model is based on the two-subunit structure from the *Paracoccus denitrificans* enzyme and contains carbon monoxide (CO) bound to heme a_3. Short (1 ps) trajectories of the enzyme were calculated, each initiated by the sudden breaking of the Fea_3−CO bond. A comparison of two sets of calculations suggests a functional mechanistic role of the covalent bond between Tyr280 and His276, the latter being one of the three histidines coordinating the copper atom CuB. In particular, the presence of this bond enhances the coupling of the CO motion to the environment and confines motion of CO on the picosecond time scale to the region close to CuB. On the time scale of a few hundred femtoseconds after dissociation, the most important movement of CO consists of rotation over ∼90° and the most favorable position for binding to CuB appears to be occupied after 300−400 fs. These results are discussed in the light of the recent suggestion that the reaction coordinate of coherent reaction dynamics of heme a_3 after photodissociation involves CO transfer to CuB (Liebl, U.; Lipowski, G.; Négrerie, M.; Lambry J.-C.; Martin, J.-L.; Vos, M. H. *Nature* **1999**, *401*, 181.).

1. Introduction

Cytochrome *c* oxidase (CcO) is the terminal enzyme in the respiratory chain of mitochondria and aerobic bacteria. It catalyzes the four-electron reduction, by soluble cytochrome *c*, of molecular oxygen to water.[1] This reaction is coupled to the generation of a trans-membrane proton gradient. The enzyme is a multisubunit integral membrane protein.[2−4] The number of subunits varies between different organisms, but only the strongly conserved subunits I and II carry the functionally important cofactors.[2] The determination of the structure of the system from the bacterium *Paracoccus denitrificans* (*P. denitrificans*)[3] and from bovine heart mitochondria[4] has provided a substantial advance in understanding its functioning on a molecular level.

The binuclear active site, where oxygen and the oxygen radical intermediates are located during the reaction, contains two cofactors, an A-type heme, heme a_3, and a copper ion, CuB. The a_3 iron and CuB are located at a distance of only ∼5 Å. Heme a_3 functions as the stable binding site for external diatomic ligands (O_2, CO, NO, etc.). Transfer of these ligands to and from heme a_3 is thought to pass via binding to CuB,[5−8] and CuB can be regarded as the "doorstep" toward the active site. The dynamics of ligand shuttling can be studied using flash photolysis of ligands from the Fe a_3. In this way, it has been shown that the transfer of CO from heme a_3 to CuB takes less than 1 ps.[9] This is substantially faster than would be expected on the basis of diffusional arguments, and therefore it was suggested that the transfer is driven by concerted motions of the constituents of the binuclear site.[9] Very recently we have demonstrated that upon dissociation of CO from heme a_3 the heme product state—the unliganded ground state—forms in a stepwise manner, thus providing a first example of coherent population dynamics in a protein system.[10] Such reaction dynamics have not been observed in other heme proteins, indicating that the specific environment of the binuclear site is involved in the motions driving this reaction. Moreover, the main step of the reaction (at ∼350 fs) occurs on the time scale expected for CO transfer to CuB in a ballistic model.[9]

Here we study the structural dynamics in the binuclear site upon CO dissociation from heme a_3 using molecular dynamics simulations. We focus on the dynamics taking place within 1 ps, and our simulations reveal substantial concerted motions on this time scale. We also investigate the role of the unusual covalent bridge between a histidine ligand of CuB and a close-lying tyrosine, which has been resolved in the difference Fourier map of the X-ray structures.[3,4] The simulations are based on a model constructed from the two-subunit X-ray structure of the *P. denitrificans* enzyme[3] (PDB file code 1AR1).[11]

2. Methods

Subunits I and II of cytochrome *c* oxidase were constructed using the molecular modelisation program CHARMM (version 24b2).[12] The initial coordinate set was taken from the two-subunit/Fv antibody fragment X-ray structure of the *P. denitrificans* enzyme.[3] The model includes 531 residues of subunit I, 256 residues of subunit II, 2 hemes (*a* and a_3), 3 copper atoms, 1 magnesium atom, 1 calcium atom and 44 structural water molecules. In addition, the interface between the protein and its environment was simulated with 14 phosphatidylcholine molecules and 1161 additional water molecules (see below). Without these additions, a stable minimized structure could not be obtained. Finally 1 CO molecule was added to the structure. Initially, it was bound to the heme a_3 iron atom, using the Fe−C bond length (1.90 Å) reported for the bovine heart cytochrome *c* oxidase complex.[4] All the simulations were performed with a

* Corresponding author. Email: vos@enstay.ensta.fr.

10.1021/jp992587d CCC: $18.00
Published on Web 11/18/1999

CuB charge equal to +1e and ferric Fe a_3 and Fe *a*, since we simulate the reduced form of the enzyme.

Hydrogen atoms were generated using the CHARMM HBUILD command and the length of the bonds with hydrogen atoms was fixed by the SHAKE algorithm.[12] Water molecules were simulated using the TIP3P model. The 1161 added water molecules are taken from the solvent coordinates of a previously published bilayer membrane simulation.[13] Added solvent molecules (439 on the periplasmic side and 722 on the matrix side) are homogeneously distributed on the polar protein surface outside the membrane region. The coordinates from the alkyl chains in the X-ray structure and CHARMM atom construction algorithms were used to generate eight phosphatidylcholine (PC) lipid molecules by superposition of their common atoms; the remaining six PC molecules were constructed near membrane hydrophobic residues. The lipid PC is used because it is ubiquitous in cell membranes, and in particular, because it is present in the four subunits model structure of the *P. denitrificans* enzyme.[14]

The model of 18062 atoms was energy minimized using 20 steps of the steepest descent algorithm followed by 2000 steps of the adapted basis Newton Raphson method.[12] The noncovalent interactions were gradually set to zero between 10 and 13 Å; their list was reactualized at 10 fs intervals and a relative dielectric constant equal to unity was applied to the entire structure. The equations of motion were numerically integrated using the Verlet algorithm[15] with a 1 fs time step during the molecular dynamic simulations.

Simulations were performed using two different starting models. In model **A** no interaction between His276 and Tyr280 was imposed, whereas in model **B** a covalent bond between His276 Nϵ_2 and Tyr280 Cϵ_2 was introduced.[3,4] A standard N−C bond length of 1.36 Å was taken; this length is compatible with the revised, His−Tyr bond containing, model structure of bovine heart CcO (PDB file code 2OCC).[11]

To prepare simulations with structure **A**, an initial heating to 30 K over 10 ps was performed with three 10 K steps. This was followed by a first equilibration at 30 K over 10 ps to gradually remove the most important thermal structural changes, predominantly near the added lipid and solvent molecules. Subsequently, a second heating from 30 to 300 K over 27 ps was achieved. Finally, a long equilibration period (110 ps) allowed us to obtain a stable starting structure to perform the simulations of the CO dissociation, as can be seen from the time evolution of the total energy, the root-mean-square difference (rmsd) between the coordinates of the current structure and the minimized structure and the temperature (Figure 1).

To generate structure **B**, the equilibrated structure **A** was used, the hydrogen atoms His276 Hϵ_2 and Tyr280 Hϵ_2 were deleted from the atom list, and the covalent bond between His276 Nϵ_2 and Tyr280 Cϵ_2 was added to the bond list. Subsequently, the same heating protocol as above was performed, but a shorter equilibration period (40 ps) was sufficient to obtain a stable structure. A general overview of the structural model and a comparison of the active site for both models is shown in Figure 2.

To simulate CO dissociation, the sudden approximation is used.[16] This method consists of deleting the Fe−C bond and simultaneous switching to the deoxy parameters. For free CO, a three-charge model was used which reproduces adequately its dipole and quadrupole moments.[17,18]

For each model (**A** and **B**), 18 independent trajectories, each of 1 ps, were run after CO dissociation from the heme a_3 iron atom. The different initial structures and velocities for each run were generated by additional trajectories of the CO-bound

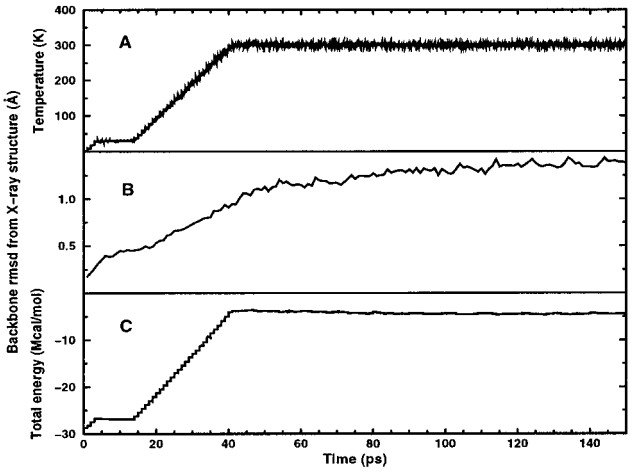

Figure 1. System time evolution during the preparing heating and equilibration phases (model **A**) (**A**) Temperature. (**B**) Backbone atoms rmsd from X-ray minimized structure. (**C**) Total energy.

structures after the equilibration, and selecting structures spaced at 1 ps. During the 1 ps CO-dissociated trajectories, the structure was saved every 10 fs and a selected number of parameters (distances between atoms and angles) was saved every 1 fs. The angle between CO and the normal of the heme is defined as the angle between the vectors $\overrightarrow{CO}$ and $\overrightarrow{CH}$, where H is the projection of C on the heme plane. The angle CuB−C−O is defined as the angle between the vectors $\overrightarrow{CuBC}$ and $\overrightarrow{CO}$.

3. Results

3.1 Pathways of CO after Dissociation. Effect of Tyr−His Bond. Throughout this study we followed the enzyme−CO complex after disruption of the heme a_3−CO bond. We emphasize the absence of an attractive potential for binding of CO to either CuB or heme a_3. Therefore we cannot directly study the ligand binding to CuB or its geminate recombination to heme a_3, but rather we investigate whether the structure reaches minima in the local potential energy surface from which likely CO binding to the cofactors is likely to occur.

Figure 2B represents the superposition of the CO-binding heme a_3−CuB active site region for model **A** and model **B** after energy minimization. Structural changes can be seen near His276 and Tyr280, but also to a minor extent on CO (Fea_3−C−O angle 178° and 174°, respectively[19]) and on CuB and its other coordinating histidines. In particular, in model **B**, the distance between the CuB atom and the heme a_3 normal is smaller by 0.4 Å as compared to that of model **A**.

Figure 3 shows the 18 final CO position for each model. For model **A**, the CO locations present a broad distribution inside the distal heme pocket. The ligands are surrounded by Trp164, Trp272, Gly275, His276, Val279, Tyr280, His326, and heme a_3. All trajectories evolved to a CO location out of the region directly between Fea_3 and CuB. The distance of the center of mass of CO to the heme plane varied from 3 to 5 Å in the different trajectories and the orientation of CO with respect to the heme normal varied over the full 180°. Close inspection indicates that the 18 1-ps CO locations can be grouped into two different clusters (with 7 and 11 members) at ∼3.7 Å distance. This suggests a weak energy barrier which can be crossed on the time scale of a picosecond for this model.

For model **B**, the evolution of CO was much more restricted and well-defined, and its motion was predominantly characterized by a rotation of ∼90°, the carbon atom rotating toward

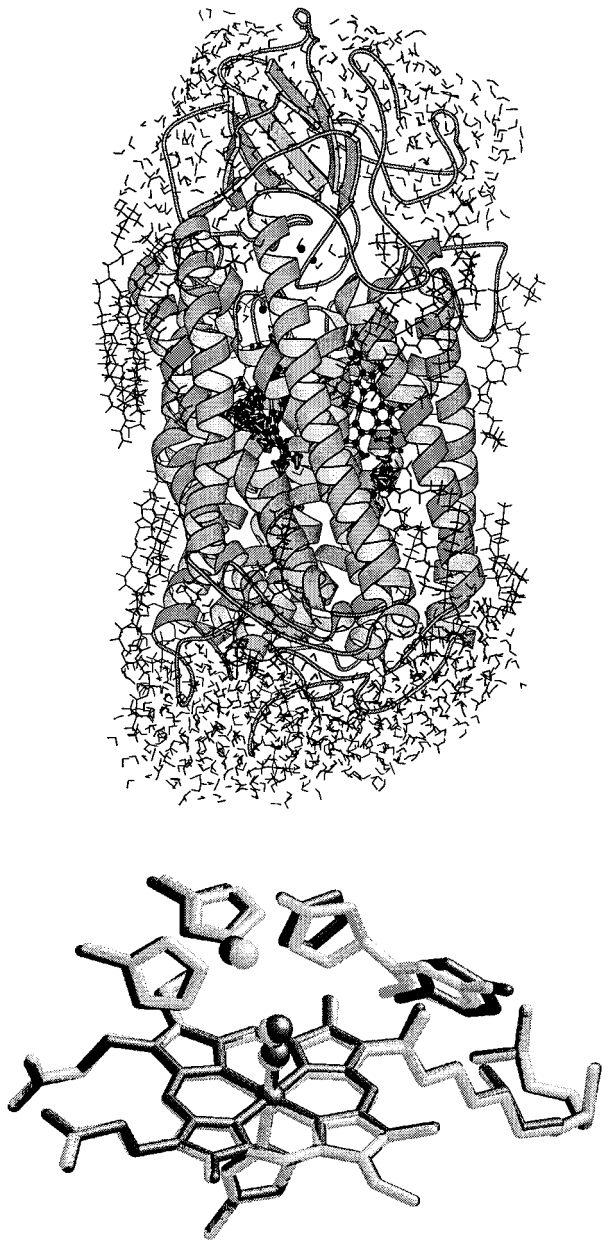

Figure 2. (**A**) Structure of the simulated system (model **B**) showing subunits I and II (ribbon representation), cofactors (ball-and-stick representation), lipid and solvent molecules (wireframe representation). (**B**) Superposition of the two minimized structural models near the heme a_3−CuB site (Model **A**: black. Model **B**: gray). The programs MOLSCRIPT[34] and RASMOL[35] were used to draw the Figures **A** and **B**, respectively.

CuB. In all final (1 ps) locations CO is surrounded by Trp272, His276, Val279, Tyr280, His325, His326, and heme a_3, directly between the Fea_3 and CuB. In particular, the distance of the center of mass of CO to the heme plane was significantly less (see also Figure 5) and more confined (2.3−3.3 Å) than for model **A** and the orientation of CO with respect to the heme normal varied only from 60 to 110°. For two trajectories, brief and reversible excursions out of this confined region (into one of the cluster regions described above for model **A**) were observed. It would appear that the link between Tyr280 and His276 "stitches" the heme pocket, thus hindering the CO to move away from the a_3 and CuB binding sites.

In the following we will analyze the dynamics of the complex more closely by looking at the time evolution of specific parameters. In the kinetics, all individual trajectories for model **B** are plotted, along with their average. For comparison the average for model **A** is also represented. Figure 4 shows the response of the configuration of heme a_3 to CO dissociation. Fea_3 is seen to move out of the heme plane toward the proximal histidine (His 396) in ∼60 fs.[20] At this time, the out-of-plane motion (0.5−0.6 Å) has a larger amplitude than the Fe−His contraction (0.3−0.4 Å, this corresponding to a ∼15% bond length decrease), hence the Fe pushes the His away from the heme. After 1 ps the remaining Fe−His contraction amounts to ∼0.1 Å. This new equilibrium value is reached in an underdamped oscillatory manner, with a frequency of ∼150 fs, corresponding well with the known frequency (∼220 cm^{-1}) of the Fe−His mode after photodissociation.[21−23] The Fe−His oscillations also show up in the Fe-heme plane motion, indicating that both motions are coupled. In similar simulations of CO dissociation from myoglobin[18] such oscillations were also seen in the Fe−heme motion, but with a somewhat longer damping time (>500 fs), consistent with results from femtosecond coherence spectroscopy on MbNO.[24]

A relaxation on a somewhat longer time scale is also apparent in the Fe−heme plane motion: the Fe−heme plane distance is significantly larger at 200−400 fs than that at 600−800 fs. This lower frequency motion is more clearly seen in the Fea−Fea_3 distance (Figure 4C), which is less modulated by the 220 cm^{-1} motion. The limited length of our trajectories (1 ps) does not allow to determine whether this motion is underdamped. The time scale of this motion roughly corresponds to that expected for the heme-doming mode (∼50 cm^{-1}) inferred from normal mode calculations of the isolated 5-coordinate heme−imidazole system.[25] We note, however, that the amplitude of this motion corresponds to only ∼0.2 Å and that the initial (0.5−0.6 Å) Fe−heme plane motion occurs on a faster time scale, presumably due to the strong mixing with the Fe−His motion.

Figure 5 shows the motion of CO with respect to the heme plane. As mentioned above, the CO translational motion is much more restricted for model **B**. Interestingly, in the C_{CO}−Fea_3 distance, the 150 fs Fe−His vibration shows up clearly for model **B**, but not for model **A**. This also points to strong correlation of the CO position with its environment, versus more uncorrelated motion in model **A**. The rotation of CO, over ∼90°, reaches its maximum in 300−400 fs; i.e., much slower than the main translation of the molecule, which occurs in ∼60 fs.

Figure 6 shows the motion of CuB. After an initial lag phase of ∼100 fs, clearly CuB moves away from the heme plane in 300−400 fs for as much as nearly 1 Å in model **B**, and far less in model **A**, where CO does not stay between Fea_3 and CuB. Thus, CuB seems to be pushed away by the rotation (and not by the initial translation) of CO. At the same time, until ∼300 fs, CuB does not strongly move with respect of the plane formed by its coordinating histidines, indicating that CuB and its immediate surroundings move in a concerted way. Interestingly, at that time (300 fs), in part (∼50%) of the trajectories, a rather abrupt increase of this distance (motion of CuB away from the heme) is seen, and actually the set of trajectories bifurcates at this moment. This splitting into two distinct groups can be seen in other parameters as well (Figure 6A).

Eventually, within 1 ps CO will bind CuB.[9] This binding is not included in our classical simulations, as the binding potential for CuB−CO was switched off. However, the CuB−CO distance and orientation as a function of time can give information about the timing of the optimal configuration for binding. Figure 7 shows the distance between CuB and the carbon and oxygen atoms of CO, as well as the CuB−C−O angle. The CuB−C

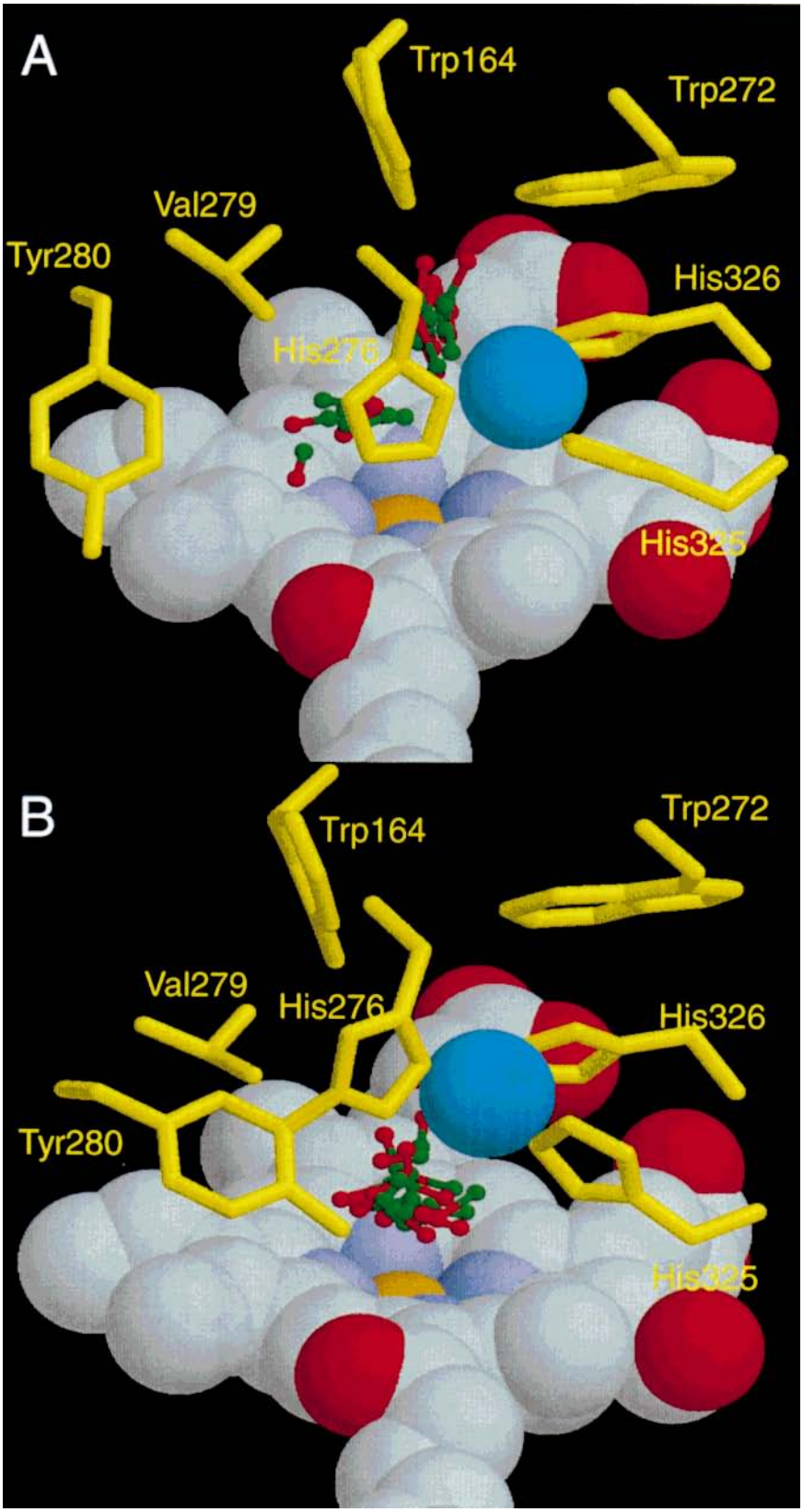

Figure 3. Final position of the CO ligands 1 ps after the dissociation from the heme a_3 iron atom. (**A**) Model **A**. (**B**) Model **B**. The spheres represent heme a_3 atoms (grey: carbon; red: oxygen; purple: nitrogen; brown: iron) and the CuB atom (blue). The CO molecules are drawn in a green (carbon atom) and red (oxygen atom) ball-and-stick model. The residues surrounding the CO molecules are drawn in yellow wireframe. The program RASMOL[35] was used to prepare the figure.

distance initially decreases to ~2.7 Å in ~60 fs by the fast "recoil" evolution of CO toward CuB; this fast contraction is reversed in the next 60 fs. At this time the CuB−O_{CO} distance is yet shorter (down to 2 Å) and the angle is still close to 180°. As only the carbon atom can be bonded to CuB, the arrangement is unfavorable for binding (the most favorable position for CO binding corresponds most likely to a small CuB−CO angle[26]). After ~150 fs, the CuB−C distance remains at 3−4 Å, but the

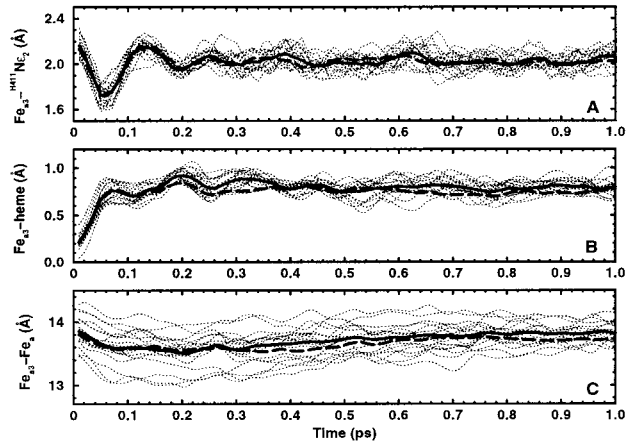

Figure 4. Time evolution, after CO dissociation, of the distance between the heme a_3 iron atom and the proximal histidine (His411) Nϵ_2 atom (A), the heme a_3 plane (B), and the heme *a* iron atom (C), respectively. Average (thick solid line) of the 18 individual trajectories (thin dotted lines) are represented for model **B**. The average for model **A** is represented as a thick dashed line.

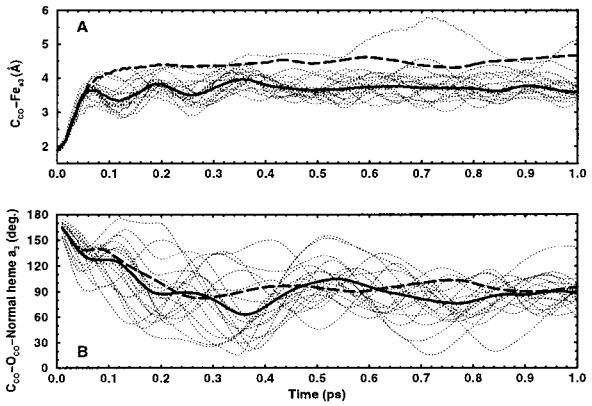

Figure 5. Time evolution, after CO dissociation, of the distance between the CO carbon atom and the heme a_3 iron atom (A) and of the angle between CO and the normal to the heme a_3 plane (this plane is determined by the average plane of the 24 heavy atoms of the heme porphyrin core).

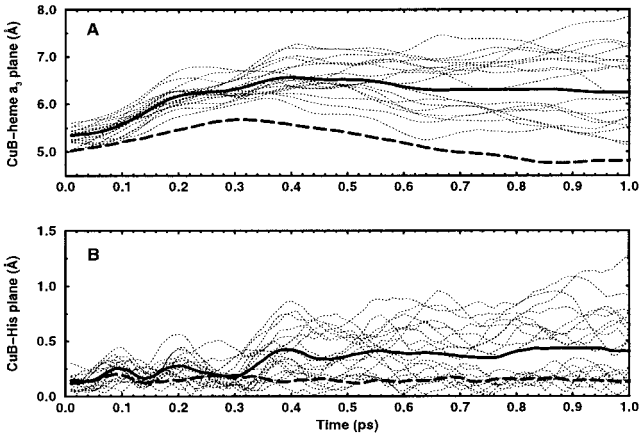

Figure 6. Time evolution, after CO dissociation, of the distance between the CuB copper atom and the heme a_3 plane (A) and the plane determined by the CuB ligands His325 Nϵ_2, His326 Nϵ_2 and His276 Nδ_1 (B), respectively. Line coding as in Figure 4.

oxygen atom rotates away, to on average a slightly larger distance and a much smaller angle which reaches, on average, a minimum at 300−400 fs; after this time it increases again.

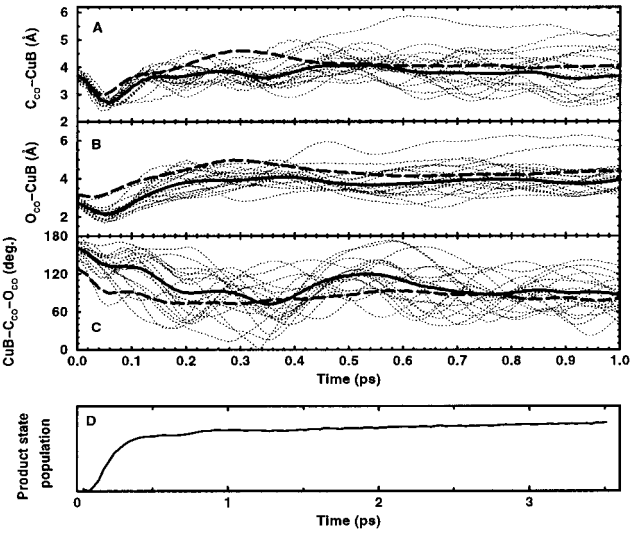

Figure 7. Time evolution, after CO dissociation, of the distance between the CuB copper atom and the CO carbon (A) and oxygen (B) atom and of the CuB−C−O angle (C). Line coding as in Figure 4. (D) population kinetics of the heme a_3 unliganded ground state after photodissociation of CO, obtained by femtosecond spectroscopy and redrawn from ref 10.

This suggests that the first favorable configuration for CO binding to CuB is reached after ∼300−400 fs.

4. Discussion

4.1 Role of Covalent Bond between Tyr280 and His276. The most recent X-ray structures of both the bovine cytochrome *c* oxidase enzyme[4] and of the *P. denitrificans* enzyme[3] point at the presence of a covalent bond between Tyr280 and His276 (*P. denitrificans* numbering), and chemical evidence for this bond has also been reported.[27] It has been suggested by several groups that such an unusual arrangement could play an important role in electron and proton transport[3,4,27−30] via modification of the redox and protonation properties of the tyrosine. However, very recent calculations indicate that the influence of cross-linking with histidine on the redox potential of tyrosine is very small.[31] As will be discussed below, our present simulations point at a *mechanical* role of the His−Tyr bond, as it rigidifies the environment of the binuclear center.

We have explored the influence of the His−Tyr bond in our simulations, by comparing two models, one in which the covalent bond was absent (model **A**) and one in which it was imposed (model **B**). The influence on the dynamics of dissociated CO is apparent in several ways. The presence of the covalent bond restricts the motion of CO to a relatively well defined pathway, where it is also more coupled to the motion of its surroundings. Moreover, it hinders CO to easily move out of the inter heme a_3−CuB space. The effect is more subtle than only closing an escape route by the covalent bond, as in model **A** (no bond), the ligand appears to move *away* from Tyr280 and His276. So it seems that the strain induced by the bond also influences the escape probability on the other side of the cavity.

Some insight in the structural basis of this observation can be gained from a comparison of the minimized structures for the two models (Figure 2B). It can be seen that the contraction of the Tyr280−His276 distance forces the copper atom CuB (coordinated by His276) toward the heme a_3 normal, and along with CuB, His325 and His326 also close in. From a different perspective, this is also seen in Figure 3. The overall effect appears to be a confinement of the entire site. The ensemble of

results thus suggest that the Tyr−His bond is functional in restricting and rigidifying the heme a_3−CuB pocket to avoid escape of CO. One might speculate on a similar role in the prevention of escape of oxygen and especially highly toxic oxygen radical reaction intermediates after thermal dissociation.

4.2. Pathway of CO motion towards CuB. The early events after CO dissociation are heme a_3 doming and ligand repulsion from iron atom. Our simulations show an ultrafast decrease of C_{CO}-CuB distance (3.7 to 2.75 Å in 60 fs). It is unlikely that CO binds to CuB directly along with this initial approaching, as the CuB−C−O angle (>120°, Figure 7C) is unfavorable for binding on this time scale. Major CO rotation takes place in a few hundred femtosecond and reaches a minimum at 300−400 fs (Figures 7C and 5B). This suggests that rotation of CO is the limiting factor for binding to CuB, and possibly that the transition zone is first reached at 300−400 fs. Such a transfer time is in agreement with the upper limit of 1 ps determined by transient infrared spectroscopy.[9,32] Moreover it is very interesting to compare this result with our recent results on photodissociation of CO from heme a_3 using femtosecond transient visible absorption spectroscopy.[10] We demonstrated that the decay of the unliganded heme a_3 to the ground state occurs in a stepwise, coherent, manner, with a first and main (80−90%) step after ∼350 fs. This time is remarkably similar to the 300−400 fs rotation time calculated here, suggesting that these two events are related. In the framework of our previous suggestion that the coherent reaction dynamics of heme a_3 are coupled to CO transfer toward CuB,[10] we propose that rotation of CO (and the concerted motion of CuB and its surroundings, see above) constitutes an essential element of the reaction coordinate motion.

As stated earlier, our present modeling does not directly include the binding of CO to CuB. One way to model this is to use a classical Landau−Zener approach, previously employed with one single reaction coordinate (Fe−ligand distance) for NO binding to myoglobin.[18,33] Our results indicate that in the present case, such modeling should minimally include not only the distance of CuB and the ligand, but also the orientation of the ligand, which substantially increases the number of model parameters. A preliminary study to explore the usefulness of such a model in this context is underway.

Acknowledgment. M.H.V. is supported by CNRS.

References and Notes

(1) Babcock, G. T.; Wikström, M. *Nature* **1992**, *356*, 301.
(2) Michel, H.; Behr, J.; Harrenga, A.; Kannt, A. *Annu. Rev. Biophys. Biomol. Struct.* **1998**, *27*, 329.
(3) Ostermeier, C.; Harrenga, A.; Ermler U.; Michel, H. *Proc. Natl. Acad. Sci. U.S.A.* **1997**, *94*, 10547.
(4) Yoshikawa, S.; Shinzawa-Itoh, K.; Nakashima, R.; Yaono, R.; Yamashita, E.; Inoue, N.; Yao, M.; Fei, M. J.; Peters Libeu, C.; Mizushima, T.; Yamaguchi, H.; Tomizaki, T.; Tsukihara, T. *Science* **1998**, *280*, 1723.
(5) Alben, J. O.; Moh, P. P.; Fiamingo, F. G.; Altschuld, R. A. *Proc. Natl. Acad. Sci. U.S.A.* **1981**, *78*, 234.
(6) Fiamingo, F. G.; Altschuld, R. A.; Moh, P. P.; Alben, J. O. *J. Biol. Chem.* **1982**, *257*, 1639.
(7) Lemon, D. D.; Calhoun, M. W.; Gennis, R. B.; Woodruff, W. H. *Biochemistry* **1993**, *32*, 11953.
(8) Verkhovsky, M. I.; Morgan, J. E.; Wikström, M. *Biochemistry* **1994**, *33*, 3079.
(9) Dyer, R. B.; Peterson, K. A.; Stoutland, P. O.; Woodruff, W. H. *Biochemistry* **1994**, *33*, 500.
(10) Liebl, U.; Lipowski, G.; Négrerie, M.; Lambry J.-C.; Martin, J.-L.; Vos, M. H. *Nature* **1999**, *401*, 181.
(11) Bernstein, F. C.; Koetzle, T. F.; Williams, G. J. B.; Meyer, E. F. Jr.; Brice, M. D.; Rodgers, J. R.; Kennard, O.; Shimanouchi, T.; Tasumi, M. *J. Mol. Biol.* **1977**, *112*, 535.
(12) Brooks, B. R.; Bruccoleri, R. E.; Olafson, B. D.; Swaminathan, S.; Karplus, M. *J. Comput. Chem.* **1983**, *4*, 187.
(13) Heller, H.; Schaefer, M.; Schulten, K. *J. of Phys. Chem.* **1993**, *97*, 8343.
(14) Iwata, S.; Ostermeier, C.; Ludwig, B.; Michel, H. *Nature* **1995**, *276*, 660.
(15) Verlet, L. *Phys. Rev.* **1967**, *159*, 98.
(16) Petrich, J. W.; Lambry, J.-C.; Kuczera, K.; Karplus, M.; Poyart, C.; Martin, J.-L. *Biochemistry* **1991**, *30*, 3975.
(17) Straub, J. E.; Karplus, M. *Chem. Phys.* **1991**, *158*, 221.
(18) Lambry, J.-C. Thesis, University of Paris-Sud, 1997.
(19) The Fea_3−C−O structure is somewhat more linear than the published CO-bound structure for the beef heart enzyme (152°).[4] It should be noted, however, that a very high resolution X-ray structure is required for accurate determination of such angles, as illustrated recently for MbCO (Kachalova, G. S.; Popov, A. N.; Bartunik, H. D. *Science* **1999**, *284*, 273).
(20) Similar times were simulated for CO dissociation from myoglobin in refs 17, 18, and Henry, E. R.; Eaton, W. A.; Hochstrasser, R. M. *Proc. Natl. Acad. Sci. U.S.A.* **1986**, *83*, 8982.
(21) Schelvis, J. P. M.; Deinum, G.; Varotsis, C. A.; Ferguson-Miller, S.; Babcock, G. T. *J. Am. Chem. Soc.* **1997**, *119*, 8409.
(22) Findsen, E. W.; Centeno, J.; Babcock, G. T.; Ondrias, M. R. *J. Am. Chem. Soc.* **1987**, *109*, 5367.
(23) Woodruff, W. H.; Einarsdóttir, Ó; Dyer, R. B.; Bagley, K. A.; Palmer, G.; Atherton, S. J.; Goldbeck, R. A.; Dawes, T. D.; Kliger, D. S. *Proc. Natl. Acad. Sci. U.S.A.* **1991**, *88*, 2588.
(24) Zhu, L.; Sage, T.; Champion, P. M. *Science* **1994**, *266*, 629.
(25) Li., X.-Y.; Zgierski, M. Z. *Chem. Phys. Lett.* **1992**, *188*, 16.
(26) In a small model molecule containing Cu−C−O where Cu is also coordinated by three nitrogen atoms (Achternbosch, M.; Apfel, J.; Fuchs, R.; Klufers, P.; Selle, A. *Z. Anorg. Allg. Chem.* **1996**, *622*, 1365) the Cu−C−O configuration is near-collinear (angle 3° in our convention).
(27) Büse, G.; Soulimane, T.; Dewor, M.; Meyer, H. E.; Blüggel, M. *Protein Sci.* **1999**, *8*, 985.
(28) Gennis, R. B.; *Biochim. Biophys. Acta* **1998**, *1365*, 241.
(29) Kanti Das, T.; Pecoraro, C.; Tomson, F. L.; Gennis, R. B.; Rousseau, D. L. *Biochemistry* **1998**, *37*, 14471.
(30) Proshlyakov, D. A.; Pressler, M. A.; Babcock, G. T. *Proc. Natl. Acad. Sci. U.S.A.* **1998**, *95*, 8020.
(31) Himo, F.; Eriksson, L. A.; Blomberg, M. R. A.; Siegbahn, P. E. M. *Int. J. Quantum Chem. Biophysics Quarterly*, in press.
(32) Dyer, R. B.; Peterson, K. A.; Stoutland, P. O.; Woodruff, W. H. *J. Am. Chem. Soc.* **1991**, *113*, 6276.
(33) Li, H.; Elber, R.; Straub, J. E. *J. Biol. Chem.* **1993**, *268*, 17908.
(34) Kraulis, P. J. *J. Appl. Crystallogr.* **1991**, *24*, 946.
(35) Sayle, R.; Milner-White, E. J. *TIBS* **1995**, *20*, 374.